CONFERENCE PRE-PRINT

THE RADIATIVE DIVERTOR AND IN/OUT ASYMMETRY IN HL-3 BY IMPURITY SEEDING WITH FULL DRIFTS

YANJIE ZHANG, KYUNGTAK LIM Nanyang Technological University Singapore, Singapore Email: yanjie.zhang@ntu.edu.sg

CHAOFENG SANG, XUELE ZHAO, CHEN ZHANG, YILIN WANG AND DEZHEN WANG Dalian University of Technology, Dalian, Liaoning, People's Republic of China

JIAXIAN LI, GUOYAO ZHENG Southwestern Institute of Physics Chengdu, Sichuan, People's Republic of China

ILYA Y SENICHENKOV, VLADIMIR A ROZHANSKY Peter the Great St. Petersburg Polytechnic University Saint Petersburg, Russian Federation

Abstract

The power exhaust on the plasma-facing comments (PFCs), especially for the divertor, is much challenging for the HL-3. Radiative divertor has been proposed for standard divertor (SD) by neon (Ne) and argon (Ar) seeding. In this work, the effects of the toroidal magnetic field direction, divertor geometry, D_2 fueling at upstream and impurity species on the divertor in/out asymmetry has been investigated, with emphasis on the impacts of full drifts. The simulation results show that: (1) More Ne particles accumulate in the divertor region with full drifts than that of without drifts. Moreover, the divertor in/out asymmetry is significantly reduced with unfavorable magnetic field (ion $B \times \nabla B$ drift is directed away from the primary X-point), while the Ne concentration in the core with unfavorable magnetic field is much severe than that of favorable magnetic field. (2) The shrinkage of dome can mitigate the capabilities of pump, significantly affecting the Ne ions distribution and the in/out asymmetry. (3) The upstream D_2 fueling can remarkably promote the impurity screening and affect the Ne distribution and then influence the in/out asymmetry. (4) The impurity screening with Ar seeding is better than that of Ne seeding However, the core radiation with Ar seeding is higher than that of Ne due to the high Ar radiative efficiency.

1. INTRODUCTION

High particle and heat fluxes deposited on the plasma-facing components (PFCs), especially on the divertor target is one of the critical challenges for the future fusion devices. For carbon (C) PFCs, intrinsic C impurity remarkably promotes the power radiation due to C is a strong radiator in the typical divertor temperature range of 10-20 eV [1]. However, the C PFCs has gradually been substituted by the tungsten (W) PFCs due to the strong erosion and high fueling retention [2]. For W PFCs, the power exhaust may be insufficient due to the neglectable intrinsic W impurity radiation in the divertor region. The radiative divertor via external low charge impurities seeding is a promising solution to control the steady-state heat flux density within 10MW/m^2 and $T_e < 5 \text{eV}$ simultaneously to avoid the melting and physical erosion of the target [3]. Recently, the simulations with full drifts have been successfully applied in ASDEX-Upgrade [4][5][6], C-Mod[7], DIII-D [8][9][10], JET [11], EAST [12], CFETR [13] and ITER [14][15]. It is found that the drifts play an important role on the divertor plasma conditions, such as the divertor in/out asymmetry [16][17][18][19], which is essential for the design and operation of future reactor devices such as ITER and DEMO. However, detailed understanding of the mechanism of the in/out asymmetry control is still necessary, e. g. the combined effects of divertor closure [20] and drifts, the impacts of upstream fueling [21] and the impurity species, e. g., nitrogen (N), neon (Ne) or argon (Ar) [4][6] [9][11][13][22].

HL-3 [23] is a copper-conductor medium size tokamak at SWIP with the key parameters as following: major radius R=1.78m, minor radius a=0.65m, elongation $\kappa \le 1.8$, triangularity $\delta \le 0.5$, plasma current $I_p=2.5-3.0$ MA and toroidal field $B_t=2.2-3.0$ T. First plasma has been successfully a chieved in 2020 [24]. It has the capability to operate with flexible divertor magnetic configurations, including standard, exact snowflake, snowflake plus and snowflake minus magnetic configuration [25], to test and qualify various advanced divertor concepts for future fusion devices.

In this work, we report our recent study of divertor in/out a symmetry, plasma detachment and impurity screening via external impurity seeding in standard divertor (SD) on HL-3. The scrape-off layer plasma simulation code package SOLPS-ITER [26] is used for the study. The paper is organized as follows: Section 2 presents a brief description of the model setup for the simulation. In Section 3, impurity gas seeding simulation with full drifts and currents activated. First, the effects of drifts on the divertor in/out a symmetry and impurity core concentration are analyzed with forward (the direction of the ion $B \times \nabla B$ points to the lower XP) and reversed (the ion $B \times \nabla B$ direction a way from the lower XP) B_t directions. Subsequently, with neon seeding, the impacts of reduced dome and the upstream D_2 fueling on the neon distribution and thus divertor in/out asymmetry with reversed B_t direction are investigated. Finally, the impact of seeding species, i.e. neon and argon, on the divertor plasma properties, impurity core accumulation and in/out a symmetry are evaluated. The conclusions and discussions are summarized in Section 4.

2. SIMULATION MODEL

In this work, the HL-3 lower single null (LSN) magnetic configuration is used, and the forward and reversed B_t directions are applied by switching the magnetic field direction. The impurity seeding simulations in SD are carried by SOLPS-ITER code package (3.0.8 version) [26], which couples the multi-fluid transport code B2.5 [27] with the kinetic neutral transport code EIRENE [28]. In the first stage, HL-3 will use CFC as plasma facing components (PFCs). The W will be considered as PFCs in the second stage following ITER's selection. Therefore, W PFCs is assumed in the present model. However, the W impurity is not considered due to: (1) the erosion of W PFCs is weak and W impurity has neglectable role on the edge plasma; (2) the high consumption of computing time and possible numerical difficulties during high-Z impurity simulation with fluid model. The D_2 fueling is located at the OMP, marked by the upper red arrow in FIG. 1(a), which may promotes the impurity screening by accelerating the plasma flow via puff-and-pump based on the DIII-D experiments [21]. The impurity gas (Ne or Ar) seeding near the outer strike point (OSP), indicated by the lower red arrows in FIG. 1(a), is performed to increase the divertor power dissipation. Electrons and ions with all ionization states (D+,Ne+ - Ne¹⁰⁺ or Ar+ - Ar¹⁸⁺) are included. The computational meshes, including the quasi-orthogonal mesh for B2.5 and the triangular mesh for EIRENE, are illustrated in FIG. 1(a).

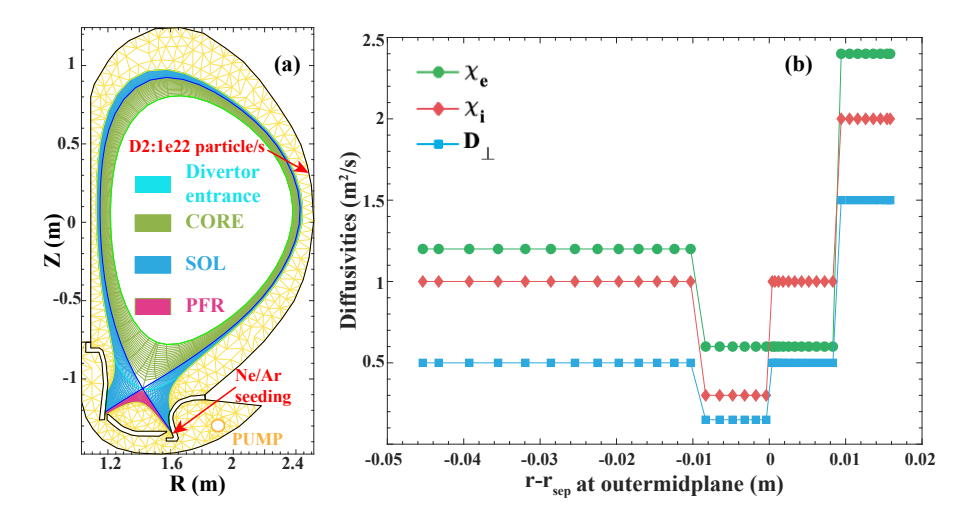


FIG. 1 (a) Sketch of the SOLPS simulation domain and wall structure. The regions of the core, SOL, PFR and the divertor entrance are indicated by different colors (the divertor entrance is taken at the X-point). (b) The imposed radial profiles of particle diffusivity D_{\perp} and electron/ion thermal diffusivity $\chi_{e,i}$ at outer mid-plane (OMP).

In the present model, at the core region, i.e. the core-edge interface (CEI, which is also known as core boundary, $r - r_{sep} = -4.75$ cm at the outer mid-plane OMP), the power across CEI is set as the energy boundary condition, $P_{SOL} = 10$ MW, equally divided between ions and electrons; the D⁺ densities is fixed to 5×10^{19} m⁻³; to control the high charge impurities density in the core, (1) during Ne seeding, the total fluxes of Ne⁸⁺ and Ne⁹⁺ are set to 5×10^{17} s⁻¹ (the positive direction towards the outermost boundary from the CEI), and the flux of Ne¹⁰⁺ is set to 5×10^{17} s⁻¹, (2) during Ar seeding, the total fluxes of Ar¹⁴⁺ and Ar¹⁵⁺ are set to -5×10^{17} s⁻¹ and Ar¹⁶⁺ flux is set to 5×10^{17} s⁻¹ (the Ar¹⁸⁺ density is low due to the low T_e at CEI, which is around 900eV), while the total fluxes of other ions and neutrals at the CEI are set to zero. The leakage boundary condition at SOL and PFR, $\Gamma = \alpha C_s n_{i,n}$, is prescribed, where C_s is the sound speed, $n_{i,n}$ is the particle density, and α is the leakage factor (1.5×10² for D, Ne and Ar neutrals and 1×10⁻³ for D, Ne and Arions). The sheath boundary (Bohm criterion) condition is

applied at the target. Other boundary conditions in the SOL/PFR/target regions are the same to Ref. [22]. When particles hit the wall, some of them are recycled as neutral atoms/molecules and returned to the simulation domain. The recycling rate (R) is set to R=0.9 in the cryo-pump and R=1 at the rest PMC. The anomalous radial transport coefficients are illustrated in FIG. 1(b), which creates a transport barrier to construct the H-mode pedestal, similar to those used for EAST [29] and ASDEX-Upgrade [6]. Only steady-state is simulated, and ELMs are not considered. The radiative power is calculated by considering the line radiation, bremsstrahlung radiation and neutral radiation. All drift terms and currents are fully turned on using the speed-up method [14] developed recently, making it possible to obtain converged results within a few months.

3. MODELLING RESULTS AND DISCUSSION

3.1. Effects of the drifts on the in-out asymmetry and impurity core accumulation

Both experiments and numerical simulation found that the divertor in-out asymmetry depends strongly on the B_t direction (drifts) without external impurity seeding. In recent EAST pure deuterium discharge experiment, it has been found that the in/out asymmetry in forward B_t direction is strong, while the in/out asymmetry in reversed B_t direction becomes nearly balance [19]. The SOLPS-ITER simulations [7][30] also observed the pronounced dependence of in/out asymmetry on drifts. With the consideration of impurity, the drifts influence the transport of the impurity, thus may have more significant impact on the divertor in/out asymmetry. To demonstrate it, simulation works have been carried out with the consideration of different drifts. With the consideration of only $E \times B$ drift, it has been found that in C divertor, the $E \times B$ drift predominate the in/out asymmetry due to the seriously in-out asymmetry of intrinsic C impurity [17][31]. With full drifts, the extrinsic impurity seeding (N, Ne) discharge also appeared remarkable in/out asymmetry, while the in/out asymmetry decreases as the size of device increases [6]. Since HL-3 is a medium size tokamak device, the drifts play a significant role on the in/out asymmetry with extrinsic impurity seeding. The comparison of the with and without $E \times B$ drift in snowflake divertor of HL-3 with Ar seeding has been made in our previous work, showing that the divertor in-out asymmetry is reversed and a ggravated in the high Ar seeding cases with forward B_t . However, the in-out asymmetry during impurity seeding on HL-3 with full drifts remains unclear.

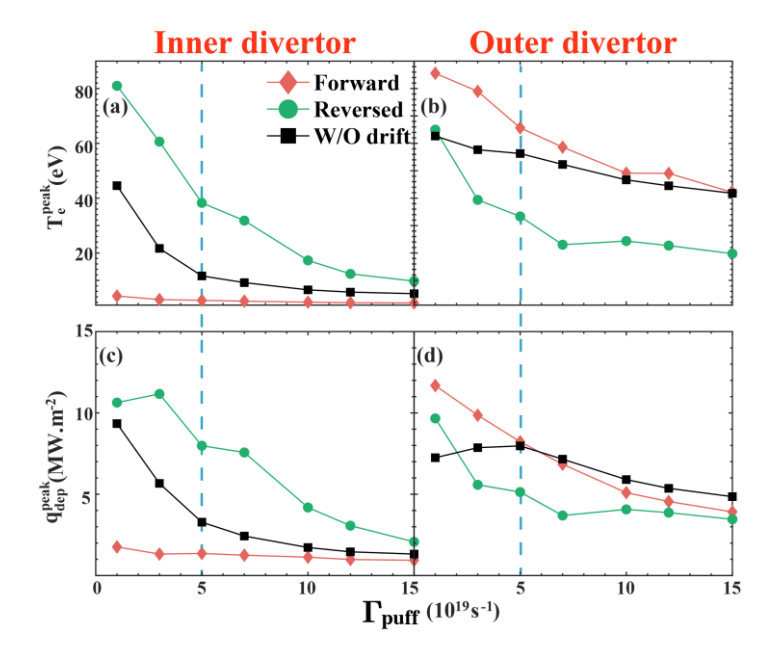


FIG. 2 The peak of electron temperature (T_e^{peak}) and deposited heat flux (q_{dep}^{peak}) in the inner divertor target (a,c) and the outer divertor target (b,d) of SD, as functions of the Ne seeding rate. The upstream D_2 fueling rates is set to 1×10^{22} particles/s. The blue dash line indicates Ne seeding rate used for detailed analysis.

To reveal the in/out asymmetry with full drifts, the Ne seeding with the combination of upstream D_2 fueling (the rates is set to 1×10^{22} particles/s by default) is selected. The T_e^{peak} and q_{dep}^{peak} on both the inner and outer divertor targets for without drifts, forward drifts and reversed drifts cases, as functions of Ne seeding rate are shown in FIG. 2. For the without drifts cases, the T_e^{peak} and q_{dep}^{peak} at inner target are slightly lower than that of outer target, which is a greement with our previous works [32]. For the forward cases, the in/out asymmetry is much

stronger, and the detachment, which is defined as $T_e^{peak} < 5 \,\mathrm{eV}$ [33], can be achieved in the inner divertor with the low Ne seeding rate (1×10^{19} Ne atoms/s). For the reversed drifts cases, the T_e^{peak} and q_{dep}^{peak} are raised in the inner divertor, while reduced in the outer divertor, indicating the inner and outer divertors become more symmetry. Unfortunately, both the inner and outer divertor are still in attached even with the high Ne seeding rate (1×10^{20} Ne atoms/s).

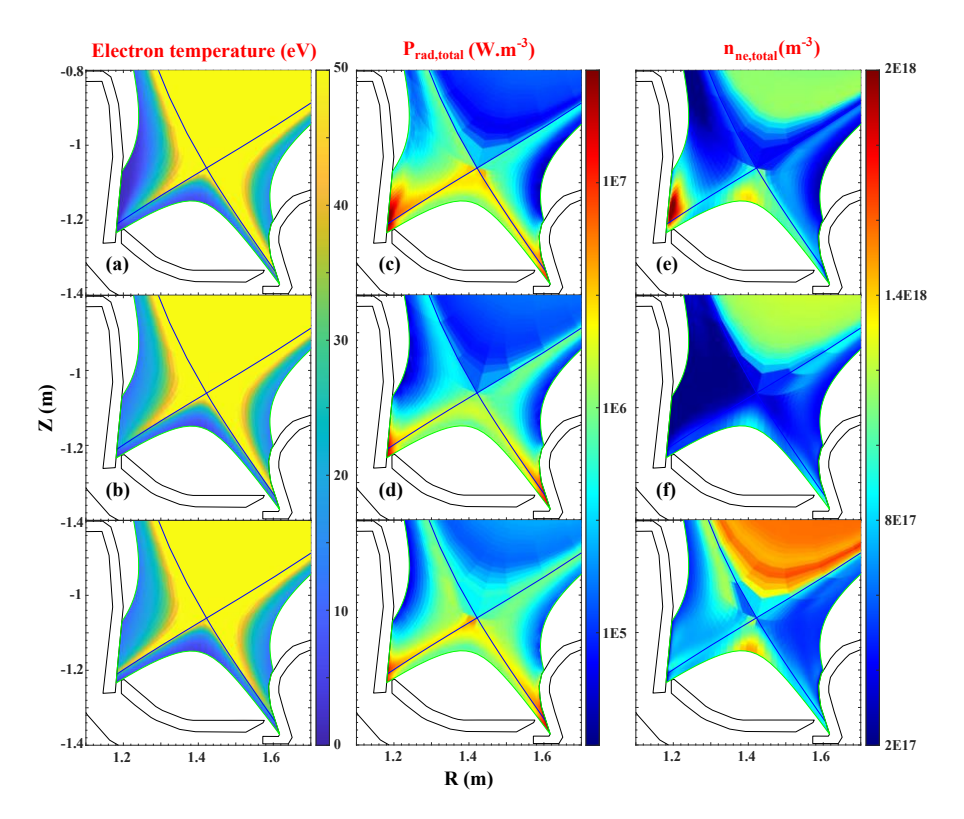


FIG. 3 The 2D contours of T_e (a-c), $P_{rad,total}$ (d-f) and total Ne density $n_{Ne,ions}$ (g-i) of forward drifts (upper), no drifts and reversed drifts (lower) cases. The Ne seeding rate is 5×10^{19} Ne atoms/s

Aiming to explain the drifts effects on the divertor plasma and in/out a symmetry, the 2D contours of T_e , total radiative power ($P_{rad,total}$) and total Ne ions density ($n_{Ne,tons}$) of no drifts, forward and reversed drifts cases with the same Ne seeding rates (5×10^{19} Ne a toms/s), marked by the blue dash lines in FIG. 2, are shown in FIG. 3. It can be seen that T_e in forward B_t of the inner divertor is much lower that of no drifts and reversed B_t cases, and it is fully detached, as illustrated in FIG. 3(a). While in the no drifts cases, T_e in the inner and outer divertor becomes to more symmetrical than that of forward case, as shown in FIG. 3(b), and the reversed case has the best in/out symmetry FIG. 3(c). From the radiation distribution, it is obvious that in forward case the high radiative power regions (HRR) mainly locates at the in the vicinity of the inner target as shown in FIG. 3(d); while in the no drifts and reversed B_t cases, the HPR primarily locates at both the inner strike point (ISP) and OSP, as shown in FIG. 3(e-f). It is notable that the radiated power around the XP in both forward and reversed drifts cases are remarkable higher than that of no drifts case. This indicates the drifts may promote the accumulation of Ne impurity in the divertor region, especially in the near-XP region. The possible reason is that drifts significant enhance the main plasma flow towards the downstream [2022 NF]. Furthermore, the Ne core accumulation in reversed B_t case is more severe than that of no drifts and forward drifts cases, as shown in FIG. 3(g-i). The explanation of the impurity core accumulation relies on the impact of drifts on the impurity transport.

3.2. Effects of the divertor geometry on edge plasma

The divertor geometry, plays important role on the divertor plasma. It has been reported that the closed divertor can promote the achievement of plasma detachment significantly by both simulations. The dome may change divertor closure, thus affecting the divertor in/out asymmetry and impurity screening. To investigate the combined effects between the drifts and divertor geometry, the dome is gradually reduced. Ne seeding with reversed drifts cases are selected due to the best in/out divertor symmetry according to previous disscusion. The albedo of cryopump is set to 0.9 by default. First only the inner dome is narrowed, and then only the outer dome is diminished, finally the dome is removed.

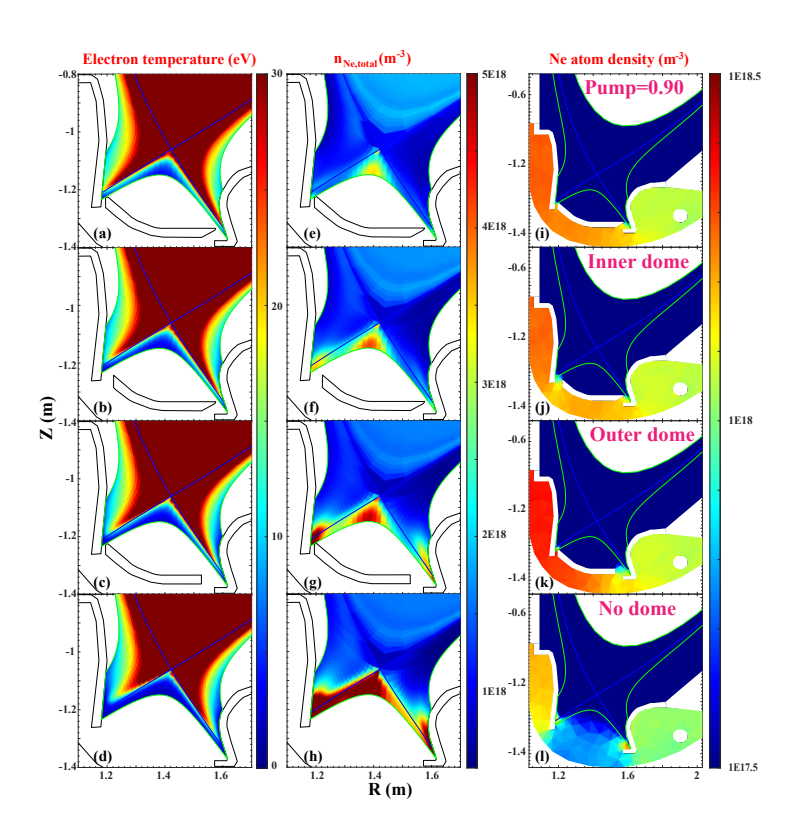


FIG. 4 The 2D contours of T_e (a-d), n_{ions} (e-h) and n_{atom} (i-f) in reversed B_t with original dome (top), inner dome modification (second row), outer dome modification (third row) and no dome modification (bottom). The Ne seeding rate is 5×10^{19} Ne atoms/s.

The 2D contours of Te, nions and natom with different dome modifications are shown in FIG. 4. It is conspicuous that the divertor Te decreases as the dome is diminished, as shown in FIG. 4(a-d). The inner Te with inner dome alteration is notably lower than that of original dome, while Te in the outer divertor is similar between the original and inner modification dome cases, as illustrated in FIG. 4(b). Comparing with the original dome case, the Te in both inner and outer divertor have a reasonably decrease, as shown in FIG. 4(c), indicating the outer dome modification is more beneficial for the divertor symmetry. For the no dome case, the Te in the inner and outer divertor significantly reduce compared with other three dome modification cases, as shown in FIG. 4(d), especially for in the vicinity of targets. The inner and outer divertor detachment achieve simultaneously for the no dome modification case. Accordingly, it is found that more Ne ions accumulate in the divertor region as dome decreases, as shown in FIG. 4(e-h), especially in PFR. To explain the difference of Ne distribution, the 2D contours of atomic Ne density are shown in FIG. 4(i-l). It demonstrates that the atomic Ne density in the vacuum decreases when dome is reduced, implying the mitigation of pump capabilities, and thus affecting the Ne ions distribution.

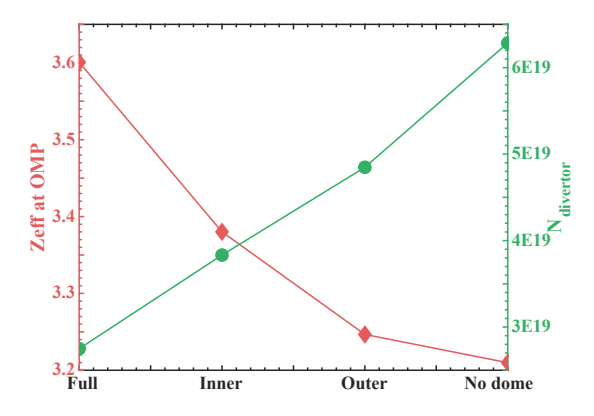


FIG. 5 The Z_{eff} at OMP (separatrix) (red line) and the total Ne particles number (including neutrals and ions) in the divertor region (the region below the divertor entrance, green line) with different size of dome. The Ne seeding rate is 5×10^{19} Ne atoms/s

The effect of dome modification on the impurity screening capacity is also assessed, the Z_{eff} at OMP (separatrix) and the total Ne particles number (including neutrals and ions) as a function of dome diminishing, as illustrated in FIG. 5. It is found that the Z_{eff} at OMP (separatrix) decreases and the total Ne particles (including neutrals and ions) in the divertor increases as the shrinkage of dome, suggesting the Ne particles are compressed from the core to the divertor region as the diminishing of dome.

3.3. Effects of the seeding impurity species on the in/out asymmetry and impurity screening

To satisfy the compatibility of detached plasma with high performance core plasma, the effects of impurity species on the plasma conditions have been studied in SD [22][34][37][38][39][40][41][42]. It is found that (1) the Ne mainly radiates around the separatrix and the XP, and easily escapes to the core due to the long mean free path and high first ionization potential (21.6 eV) [42]. (2) The Ar can simultaneously enhance the divertor and core radiation due to the low first ionization potential (15.8 eV) and high radiative efficiency, it may be trouble for the severely degradation of the core plasma performance [41]. To further study the impurity species effects on in/out asymmetry and impurity transport with forward and reversed drifts, a statistical analysis of the in/out asymmetry is shown in FIG. 6. It is found that the both the T_e and T_e and T_e in/out asymmetry for forward drifts with both Ne and Ar seeding are much intense, while the T_e and T_e and T_e in/out asymmetry for the reversed drifts is more balanced with Ne or Ar seeding, which is a greement with Ref. [16]. However, there is no notable difference of in/out asymmetry between Ne and Ar seeding.

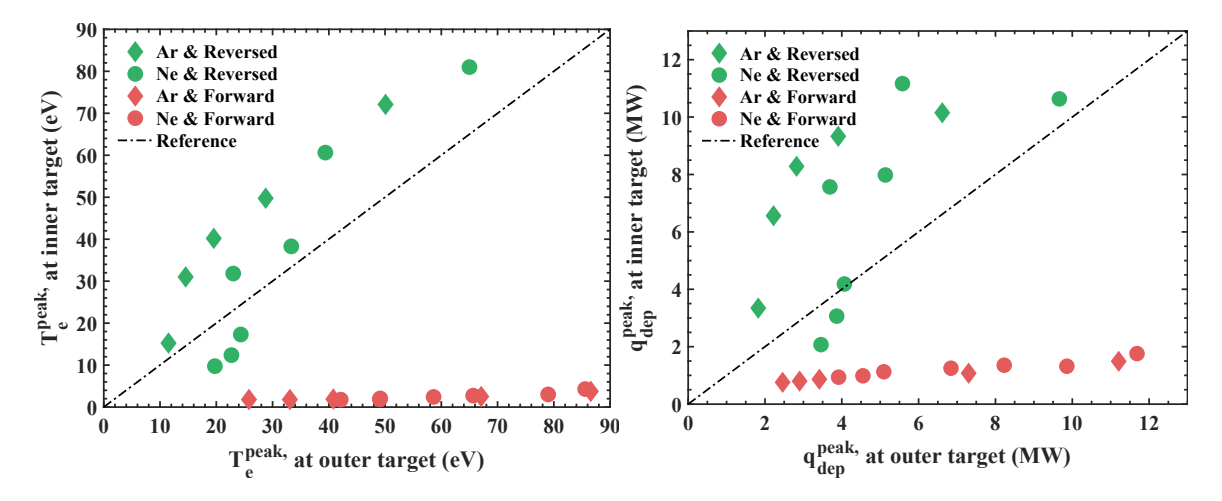


FIG. 6 Comparison of T_e^{peak} (a) and q_{dep}^{peak} (b) between inner and outer divertor for forward (red) and reversed (green) drifts with Ne (diamond marker) and Ar (circle marker) seeding.

To deeply explore the impurity on the divertor plasma conditions with full drifts, the 2D contours of T_e , $P_{rad,total}$ and n_{imp} with Ne (upper) and Ar (lower) seeding for reversed drifts with same puffing rate (Ne or Ar seeding rate is 5×10^{19} atoms/sand the upstream D₂ fueling rate is 1×10^{22} D molecules/s) are shown in FIG. 15. It is clear that the T_e in the divertor with Ar seeding is lower than that of Ne seeding, as shown in FIG. 15(a-b), which can be explained by the high Ar radiative efficiency. Accordingly, the high radiation power regions (>10MW/m³, HRPRs) with Ar seeding are more extended than that of Ne seeding, as illustrated in FIG. 15(c-d). The impurity screening with Ar seeding is much better than that of Ne seeding, and the total Ne ions density in the core is more than 2 times higher than the total Ar ions density, as shown in FIG. 15(e-f).

4. SUMMARY AND CONCLUSIONS

Modeling of SD on HL-3 with the SOLPS-ITER code has been carried out to analyze the effects of the toroidal magnetic field direction, divertor geometry, D_2 fueling at upstream and impurity species on the divertor in/out asymmetry and impurity screening, with emphasis on the impacts of full drifts. After methodically Ne puffing rate scan for forward, no and reversed drifts, dome modification, upstream D_2 fueling rate scan and Ne/Ar seeding rate scan for forward and reversed drifts, it is obtained that:

- By comparing the Ne seeding cases for forward, no and reversed drifts in SD, it is shown that drifts can remarkably enhance the main plasma conditions. More Ne particles are compressed to the divertor for drifts case than that of no drifts case due to the increase of D^+ flux in the core by drifts. Moreover, the reversed drifts cases have a better in/out asymmetry, while the in/out asymmetry for the forward drift cases are much intense due to the combined effects between divertor geometry and the $E \times B$ drift. However, the core concentration for the reversed drifts cases are severe due to strong diamagnetic inflow around the XP.
- The effects of dome modification on the in/out asymmetry and impurity screening are investigated. It is found that the shrinkage of dome can mitigate the pump capabilities, significantly affecting the Ne ions distribution and the in/out asymmetry. Moreover, the outer dome shrinkage is more efficient on the divertor Ne compression due to the associated effects between drifts and divertor geometry.
- By the D2 fueling at upstream scan for reversed drifts with fixed Ne seeding (5×1019 Ne atoms/s), it demonstrates that the upstream D2 fueling can remarkably benefit the impurity screening and a ffect the Ne distribution and then influence the in/out asymmetry.
- The core radiation for reversed drifts with Ne or Ar seeding is higher than that of forward drifts due to the strong diamagnetic inflow drives more impurities to the core region for the reversed drifts. Additionally, the impurity screening with Ar seeding is better than that of Ne seeding. However, the core radiation with Ar seeding is higher than that of Ne due to the high radiative efficiency of Ar.

This work demonstrates and explains the remarkably effects of drifts, divertor geometry, upstream D_2 fueling and impurity species (Ne or Ar) on the in/out asymmetry and divertor impurity screening in HL-3 of SD. However, some issues remain to be investigated: (1) the combined effects between the intrinsic carbon impurity and extrinsic impurity on the plasma condition with full drifts activated in SD. (2) the assessment of sputtering tungsten impurities in SD and snowflake divertor; (3) snowflake radiative divertor with active full drifts in HL-3.

ACKNOWLEDGEMENTS

This work was supported by the National Natural Science Foundation of China under Grant No. 12235002, National MCF energy R&D Program No. 2024YFE03160000.

REFERENCES

- [1] Sang C et al 2018 Phys. Plasmas 25 072511
- [2] Pitts R A et al 2019 Nucl. Mater. Energy 20 100696
- [3] Soukhanovskii V A et al 2018 Nucl. Fusion 58 036018
- [4] Senichenkov I Y et al 2019 Plasma Phys. Control. Fusion 61 045013
- [5] Senichenkov I Y et al 2021 Plasma Phys. Control. Fusion 63 055011
- [6] Rozhansky V et al 2021 Nucl. Fusion **61** 126073
- [7] Dekeyser W et al 2017 Nucl. Mater. Energy 12 899–907
- [8] Meier E T et al 2016 Plasma Phys. Control. Fusion 58 125012
- [9] Casali L et al 2022 Nucl. Fusion **62** 026021
- [10] Maurizio R et al 2021 Nucl. Fusion **61** 116042
- [11] Kaveeva E et al 2021 Nucl. Mater. Energy 28 101030
- [12] Jia G et al 2022 Nucl. Fusion **62** 056005
- [13] Si H et al 2021 Nucl. Fusion 0-20
- [14] Kaveeva E et al 2018 Nucl. Fusion 2018-July 1452-5
- [15] Kaveeva E et al 2020 Nucl. Fusion 60
- [16] Liu J B et al 2016 Nucl. Fusion **56** 066006
- [17] Du H et al 2017 Nucl. Fusion **57** 116022
- [18] Dekeyser W et al 2017 Nucl. Mater. Energy 12 899–907
- [19] Liu J B B et al 2019 Nucl. Fusion **59** 126046
- [20] Sang C et al 2017 Nucl. Fusion 57 056043
- [21] Petrie T W et al 2008 Nucl. Fusion 48 045010
- [22] Sytova E et al 2019 Nucl. Mater. Energy 19 72–8
- [23] Zheng G Y et al 2016 Nucl. Fusion **56** 126013

IAEA-CN-316/P5-3289

- [24] Duan X et al 2021 Nucl. Fusion
- [25] Li J X et al 2018 Fusion Eng. Des. 131 135–40
- [26] Bonnin X et al 2016 Plasma Fusion Res. 11 1403102–1403102
- [27] Schneider R et al 2006 Contrib. to Plasma Phys. 46 3-191
- [28] Reiter D et al 2005 Fusion Sci. Technol. 47 172–86
- [29] Sang C et al 2016 Nucl. Fusion **56** 106018
- [30] Pan O et al 2020 Plasma Phys. Control. Fusion 62 045005
- [31] Du H et al 2020 Nucl. Mater. Energy 22 100719
- [32] Zhang Y et al 2020 Nucl. Mater. Energy 25 100803
- [33] Sang C et al 2021 Nucl. Fusion **61** 016022
- [34] Hitzler F et al 2020 Plasma Phys. Control. Fusion 62 085013
- [35] Rozhansky V et al 2021 Plasma Phys. Control. Fusion 63 015012
- [36] Guo H Y et al 2019 Nucl. Fusion **59** 086054
- [37] Kallenbach A et al 2013 Plasma Phys. Control. Fusion 55 124041
- [38] Bernert M et al 2017 Nucl. Mater. Energy 12 111-8
- [39] Wang H Q et al 2017 Nucl. Mater. Energy 12 942-7
- [40] Liu X J et al 2017 Phys. Plasmas 24 122509
- [41] Yang Z et al 2017 Phys. Plasmas 24 012503
- [42] Senichenkov I Y et al 2019 Plasma Phys. Control. Fusion 61 045013